Journal of King Saud University - Science 36 (2024) 103179

HOSTED BY

Contents lists available at ScienceDirect

Journal of King Saud University - Science

journal homepage: www.sciencedirect.com

Waste polyethylene terephthalate plastic derived Zn-MOF for high performance supercapacitor application

Abdullah M. Al-Enizi *, Ayman Nafady, Nouf B. Alanazi, Meera Moydeen Abdulhameed, Shoyebmohamad F. Shaikh

Department of Chemistry, College of Sciences, King Saud University, P.O. Box No. 2455, Riyadh 11451, Saudi Arabia

ARTICLE INFO

Keywords:
Waste PET plastics
Organic linker
MOFs
Energy
Supercapacitors
Environmental remediation

ABSTRACT

A simple chemical approach was used to prepare Zn-MOF or MOF-5 derived from polyethylene terephthalate bottles for supercapacitor applications. The morphology, and structure of PET-derived MOFs were characterized using various techniques, including scanning electron microscopy, transmission electron microscopy, X-ray diffraction, thermogravimetric analysis, fourier transform infrared spectroscopy, and BET surface area and nitrogen adsorption/desorption analysis. The BET surface area of MOF-5 was determined to be 88 m^2g^{-1} and N2 adsorption–desorption analysis, showed the type-IV isotherms and suggest the existence of capillary condensation within the meso- and micropore structures. An excellent specific capacitance ranging from 341 to 191 F g^{-1} recorded form the scan rate of 2–200 mV s^{-1} by CV for Zn-MOF. Moreover, the highest specific capacitance 353 F g^{-1} calculated at 0.5 A/g current density. The highest value of specific capacitance Cs 353 F g^{-1} was found for lowest current density of 0.5 A/g. An excellent cyclic stability was obtained after running 2000 cyclic runs at a scan rate of 50 mV s^{-1}. The small semicircle of EIS plot exhibits superior electrochemical performance of the Zn-MOF. The waste PET plastic derived Zn-MOF showed an excellent supercapacitor performance which can be utilized in energy storage applications. This approach not only facilitates environmental remediation but also offers a valuable organic linker for energy material synthesis.

1. Introduction

The origin of PET can be traced back to the mid-1940s when they were first synthesized by DuPont chemists. Since then, PET has been extensively utilized in various domains such as textiles, packaging, carpeting, and single-use beverage bottles (Sousa et al., 2021; Song et al., 2022). Currently, the global consumption of PET is estimated to be between 50 and 60 million tons per year and is steadily increasing. However, the disposal of non-biodegradable PET products as waste after their useful life results in severe environmental pollution and resource depletion (Volanti et al., 2019). Therefore, there is an urgent need to develop cost-effective and eco-friendly methods for recycling PET waste to preserve resources and the environment. Extensive research has been conducted on the recycling of PET waste as a means of addressing the issue of unsustainable disposal methods such as landfill and incineration (Asensio et al., 2020). These methods are not in line with the principles of circular economy, which prioritize recyclability and sustainability, and may lead to resource depletion and secondary pollution. In contrast, chemical recycling has emerged as a more feasible option for PET waste management. This process involves depolymerization, which breaks down the PET chain into its building units, resulting in the production of useful products such as monomers, oils, and chemicals. Furthermore, the predominant constituent of PET depolymerization, namely BDC, serves as the principal organic ligand for numerous crystalline porous architectures. Consequently, the transformation of discarded PET into MOFs represents a feasible and promising approach. The novel application of waste PET for MOFs synthesis will enable the development of a high-value end-use market for PET wastes (Ubaidullah et al., 2020). Recovering BDC from waste PET would be a practical way to recycle garbage while receiving an economic benefit and helping to save the environment.

MOFs have a diverse range of applications, including wastewater purification, catalysis, chemical sensing, gas storage, and separation (Annamalai et al., 2022). The creation of MOFs involves the close association of inorganic and organic components to form open frameworks. The presence of inorganic constituents can create metal sites that

* Corresponding author.
E-mail address: amenizi@ksu.edu.sa (A.M. Al-Enizi).

https://doi.org/10.1016/j.jksus.2024.103179
Received 5 November 2023; Received in revised form 4 March 2024; Accepted 21 March 2024
Available online 22 March 2024

induce coordination, which may result in regioselectivity and selective shaping or sizing of guest molecules or reaction intermediates. The rationale for the controlled synthesis of MOFs is based on the methodical organization and well-defined environmental conditions of metal centers within pore channels. The MOFs framework can display remarkable versatility in design due to the integration of interchangeable linkers with varying geometries and functions, in addition to coordinating metal ions. This enables precise regulation of pore or channel size, surface area, and metal site type. MOF-5, a Zn-based MOF synthesized using BDC, is a prominent example among the extensively researched MOFs. The origins of MOF-5 can be traced back to 1999. This particular metal–organic framework comprises a cubic network of Zn4O units that are linked by linear BDC ligands (Biserčić et al., 2019). Due to its exceptional durability and reversible hydrogen adsorption kinetics, MOF-5 has been the focus of extensive research. Researchers have employed a sequential process involving in the depolymerization process of PET into BDC, followed by the combination of BDC with metal salts, to develop various MOFs. Examples of such MOFs include MIL-53 (Cr, Al, Ga) (Lo et al., 2016), MIL-101(Cr) (Iacomi et al., 2022), MIL-47 (V) (Zorainy et al., 2022), Ni-MOF (Zorainy et al., 2022), and UiO-66(Zr) (Kandiah et al., 2010). PET bottles have been employed as a viable source of linkers for the synthesis of MOFs. This involves the depolymerization process of PET into BDC under rigorous experimental conditions, including elevated temperatures, prolonged reaction times, and the use of acid/base catalysts.

Recently, Deleu et al. has proposed a one-pot approach for synthesizing MIL-53(Al) and MIL-47(V) by using the combination of metal salts and PET waste in a microwave oven (Deleu et al., 2016). Cho et al. demonstrated that the direct recycling process of PET waste for the fabrication of MIL-53(Al) using a one-pot hydrothermal reaction at 220 °C in self-generated pressure (Cho et al., 2021). Rajagopal et al. reported that the waste PET bottles as a linker source for MOF synthesis. The PET underwent depolymerization into BDC through a process of microwave-assisted alkaline procedure, and the purified BDC was subsequently reacted with zinc acetate to form MOF 5 (Manju et al., 2013). Similarly, Al-Enizi et al. reported that the depolymerized waste PET bottles into BDC via hydrothermal reaction in a high-pressure reactor, and the BDC was coordinated with Ni^{+2} to produce Ni-MOF. The conversion of PET into BDC typically necessitates severe experimental conditions, such as high temperatures, long reaction times, and the presence of acid or base catalysts (Al-Enizi et al., 2020). Notably, Ruoff et al. discussed the scientific and economic significance of recycling waste PET into high-value PET-based MOFs, which can be further transformed into porous carbon for green energy storage application (Li et al., 2023). These challenges represent significant impediments to the widespread manufacture and potential utilization of MOFs derived from PET.

The present investigation proposes a novel approach for the direct recycling of waste PET bottles into MOF-5 *via* a solvothermal process, without the use of catalysts. The resultant MOF-5 derived materials is subsequently employed as an active material for supercapacitor applications. The process entails the reaction of PET blocks and zinc nitrate hexahydrate in a one-pot solvothermal process, employing DMF as the solvent. This results in the complete conversion of BDC into MOF-5, as depicted in Scheme 1.

2. Experimental details

2.1. Materials

In the synthesis of the nanocomposite, analytical-grade reagents were employed without any further refinement. The chemicals utilized in the study included $Zn(NO_3)_2{\cdot}6H_2O$, $Co(NO_3)_2.6H_2O$, ethylene glycol, potassium hydroxide, N, N-dimethyl formamide, and benzene-1,4-dicarboxylic acid. The purity of the chemicals used varied, with $Zn(NO_3)_2{\cdot}6H_2O$ exhibiting purity of 98 %, $Co(NO_3)_2.6H_2O$ exhibiting purity of 99.9 %, ethylene glycol exhibiting purity of 99.8 %, potassium hydroxide exhibiting a purity greater than 85 %, N, N-dimethyl formamide exhibiting a purity of 99 %, and benzene-1,4-dicarboxylic acid being derived from waste PET bottles. The chemical substances were procured from the commercial suppliers' Sigma Aldrich and Acros Organics.

2.2. Depolymerization of waste PET plastic to produce organic linker

The present investigation involved the collection of PET plastic waste

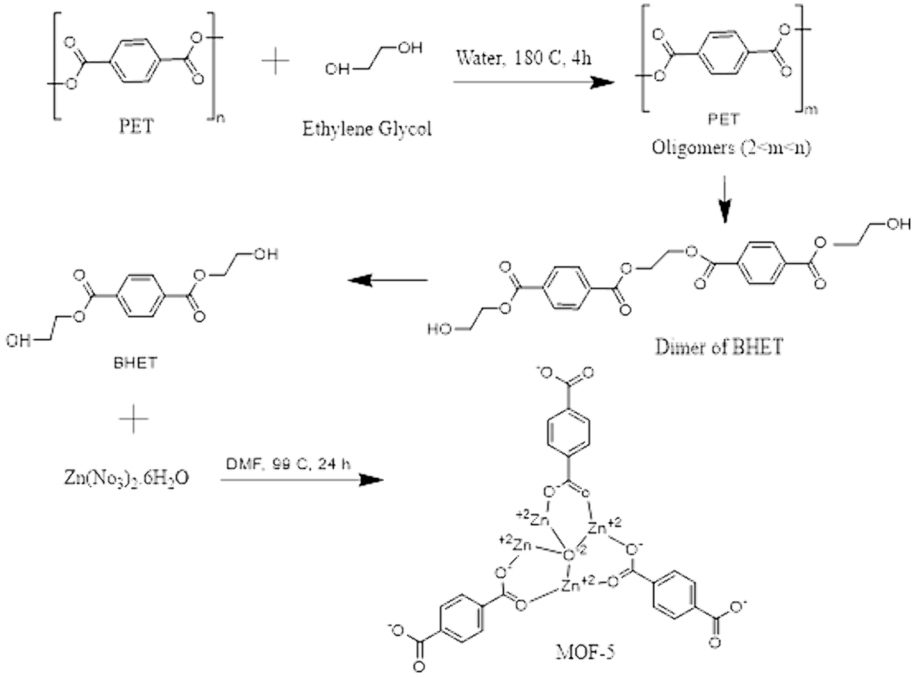

Scheme 1. Perusal synthesis reaction mechanism of MOF-5.

from the trash and its subsequent purification through an extensive washing procedure utilizing distilled water. Briefly, 1 g of this PET plastic waste was used as starting material in a Teflon auto-clave reactor with a volume of 150 ml. The reactor was filled with 20 ml of EG and 30 ml of double distilled water and subjected to a temperature of 180 °C for 5 h. Following the reaction, the reactor was permitted to cool to ambient temperature (27 °C). The resultant products were then subjected to two rounds of ethanol washing and centrifugation, then subjected to a drying process at a temperature of 100 °C for 24 h.

2.3. Synthesis of MOF-5 using PET as an organic linker source

The reagents were utilized without undergoing any further purification. The experiments were conducted in a Teflon reactor autoclave, as previously described in the depolymerization process of waste PET bottles into isolated and purified BDC. Subsequently, the BDC was combined with metal salts in a second step to form MOFs. In the MOF-5 synthesis procedure, 0.4425 g (2.67 mmol) of BDC as organic linker, and 2.095 g (8 mmol) of Zinc nitrate hexahydrate precursor (Zn $(No_3)_2{\cdot}6H_2O$) metal salt was introduced into an autoclave. Following this, 30 ml of DMF solvent was added to the reaction mixture, which was then maintained in an oven at 99 °C for 24 h. Upon cooling the reaction mixture to ambient temperature, the crystals obtained were subjected to filtration using DMF and a Buchner funnel. Subsequently, the crystals were subjected to drying in an oven at 40 °C for 10 h. The MOF-5 was activated through calcination at 450 °C for 8 h in an inert nitrogen environment and the resultant product was referred to as MOF-5. The characterization details have been provided in supplementary information as S-1 and S 1.1.

3. Result and discussion

3.1. Morphological architecture

The utilization of scanning electron microscopy (SEM) is a highly effective imaging technique that enables the acquisition of high-resolution, three-dimensional images of a sample's surface. This technique involves the scanning of a focused electron beam over the sample's surface and the collection of signals generated by the interaction between the beam and the sample to produce an image (Lewczuk and Szyryńska, 2021). In the case of MOF-5, a crystalline material, SEM can be employed to reveal the surface morphology and structure of the crystals. The study conducted on MOF-5 demonstrated that the particles exhibit mixed shapes of the agglomerated type of morphological structure. Furthermore, the study determined that the particle diameter of MOF-5 ranged from 28.3 to 88.9 nm, as illustrated in Fig. 1 (a). The morphology of MOF-5 crystals was investigated using Transmission Electron Microscopy. The analysis revealed the presence of hexagonal, pyramidal, and spherical particles, with an average size ranging from 13.513 to 129.199 nm, as illustrated in Fig. 1 (b). The chemical composition of the synthesized MOF-5 was determined using energy-dispersive X-ray (EDX) spectroscopy, as depicted in Fig. 1 (c). The EDX signals from Zinc, Carbon, and Oxygen atoms were found to be prominent and distinct. The results indicated a high percentage of Carbon content (Atomic % = 55.67), followed by oxygen percentage (Atomic % = 29.42) and Zinc atom with a percentage (Atomic % =14.91), respectively (Vellingiri et al., 2018). Elemental mapping can be accomplished by utilizing an electron beam scanning technique, which facilitates the collection of X-ray signals that show individual elements' distribution within the MOF-5 framework. These maps offer considerable analytical advantages by allowing for the visualization of the elemental composition and distribution within the material. In the case of MOF-5, the elemental constituents Zn, C, and S are respectively represented by the colors green, red, and blue as shown in Fig. 1 (d).

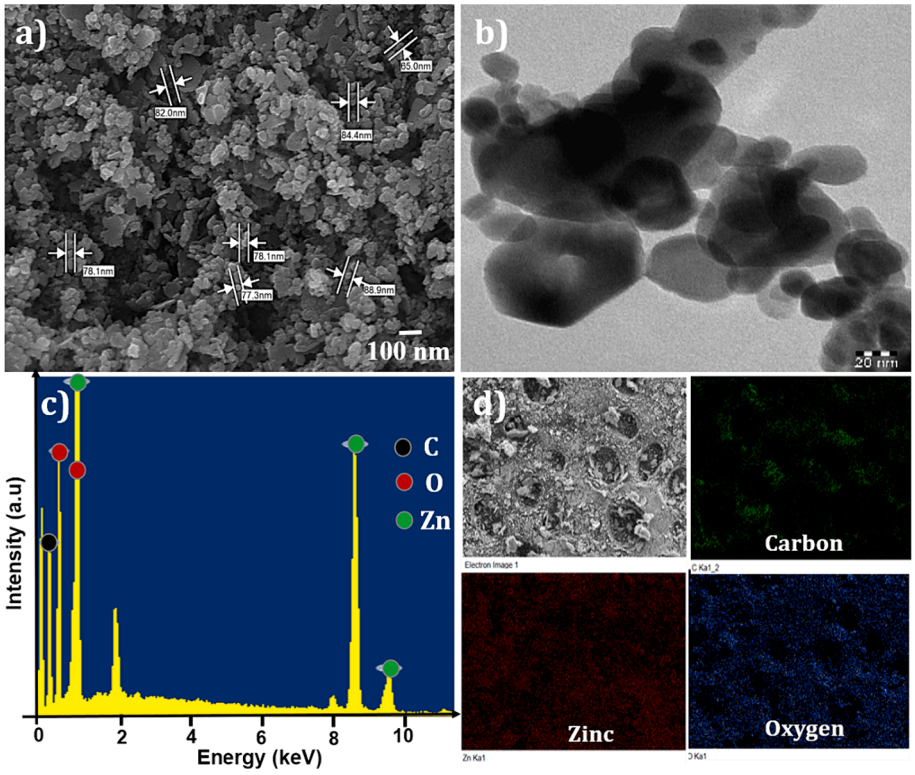

Fig. 1. A) scanning electron microscope, b) transmission electron micrographs, c) energy dispersive x-ray spectroscopic micrographs, and d) the colored images show the distribution of elemental mapping throughout the composites. c, zn, and o of mof-5.

Additionally, the elemental maps of MOF-5 demonstrate that the incorporated particles are uniformly distributed throughout the material.

3.2. Structural elucidation

In XRD analysis, the sample is exposed to an X-ray beam, and the resultant scattered X-rays are subsequently detected and analyzed to determine the diffraction pattern. This pattern serves as a unique identifier of the crystal structure and is characterized by a series of diffraction peaks. The XRD pattern of MOF-5 demonstrated the well-defined diffraction peaks that correspond to the atomic arrangement within the crystal lattice. These peaks are a result of the constructive interference between X-rays that are scattered by the atoms present in the crystal. The positions, intensities, and shapes of these peaks provide valuable insights into the crystal structure and properties of MOF-5. Fig. 2 (a) displays the XRD patterns of the MOF-5 before and after calcination was prepared. The observed XRD features that are characteristic of the synthesized materials are consistent with those that have been previously reported in the literature, stipulating the successful formation of MOF-5. The primary peaks of MOF-5 were observed at two theta = 6.8°, 9.7°, 13.7°, and 15.4°, and sharp peaks below 10° were observed for MOF-5, indicating high crystallinity of the catalysts (Kumar and Masram, 2021). Additionally, the presence of a trace amount of free ZnO (JCPDS NO. 36-1451) in the MOF-5 frameworks was confirmed by the small peak that appeared around 30–40° (two thetas). The XRD pattern of MOF-5, as illustrated in Fig. 2 (a), exhibits two minor peaks at two theta angles of 10.4 and 12.4°. The observed peaks are ascribed to the structural alterations in MOF-5 that occur during the catalyst preparation process, as documented in prior research (Zhao et al., 2012). In XRD analysis, before calcination of MOF-5 shown low intensity of the peaks is suggestive of a limited degree of crystallinity. Nevertheless, following calcination, the peaks become more pronounced and intense, indicating a high degree of crystallinity. Additionally, the lack of impurity peaks serves to authenticate the sample's high purity. Fig. 2 (b) illustrates the FTIR spectrum of MOF-5. The absorption bands detected within the range of 3500–3200 cm^{-1} are attributed to the stretching vibrations of water molecules (Sarwar et al., 2022). The absorption bands located at 1630.5 and 1475.2 cm^{-1} correspond to the stretching vibrations and asymmetric stretching vibrations of the carboxylate groups in the BDC ligand, respectively (Asadevi et al., 2022). The metal oxide band is observed within the range of 801.3–758.3 cm^{-1}. It is noteworthy that the FTIR spectra do not exhibit the characteristic peaks of protonated carboxyl groups (1715.5–1680.3 cm^{-1}), which indicates the complete deprotonation of the BDC during the reaction and its function as a bridging ligand in the formation of MOF-5 (Xu et al., 2019).

3.3. X-ray photoelectron spectroscopic studies

XPS is a highly effective analytical technique employed for the examination of the surface chemistry and electronic states of MOFs. The elemental composition, oxidation states, and chemical bonding present within MOFs can be effectively analyzed using XPS, providing valuable insights. The XPS survey spectra of MOF-5, as illustrated in Fig. 3 (a), confirm the presence of C, O, and Zn elements. Moreover, Fig. 3 (b) displays two prominent peaks located at 1022 and 1046 eV, which correspond to 2P3/2 and 2P1/2 of Zn, respectively. These values are consistent with the previously reported values for Zn^{2+} (Ubaidullah et al., 2021). The high-resolution spectrum of O1s at 530.2 eV suggests the presence of lattice oxygen in ZnO (Fig. 3 (c)). Additionally, Fig. 3 (d) demonstrated the C 1 s XPS signal detected at 284.8 eV is attributed to the C–C bond, as reported in reference (Al-Enizi et al., 2020). These observations provide convincing evidence for the successful synthesis of MOF-5, as indicated by the characterization results of the materials.

3.4. Thermogravimetric analysis of MOF-5

The thermogravimetric analysis conducted on MOF-5 has revealed the presence of two distinct phases of weight loss that occur at temperatures below 300 °C. It is plausible that these phases are a result of the elimination of physically adsorbed moisture, gases, and DMF from the pores of MOF-5. Additionally, an extra phase of weight loss is observed between 400 and 500 °C, which is accompanied by the removal of the BDC ligand and the conversion of MOF-5 to ZnO (Gu et al., 2010). These findings suggest that the framework is stable and uncontaminated, as illustrated in Fig. 4.

3.5. BET surface area and pore size analysis

The BET multipoint equation was employed to calculate the BET surface area, and pore size of the material. Before analysis, the samples underwent degassing at 200 °C for 24 h to eliminate any contaminants, including water vapor and adsorbed gases. The surface area and porosity of the samples were subsequently assessed by subjecting them to analyze relative pressure across a wide range to generate Nitrogen adsorption–desorption isotherms (Ding et al., 2001). The BET method, a widely accepted standard procedure for determining the surface area of fine powders and porous materials, was utilized. The specific surface area of MOF-5 was determined to be 88 m^2g^{-1}. According to the findings of the N_2 adsorption–desorption analysis, the type-IV isotherms present suggest the existence of capillary condensation within the meso- and micropore structures (Al-Enizi et al., 2020). The initial portions of the isotherms display a curved knee, indicating the initial adsorption of a few monolayers. Furthermore, the low slope area of the isotherms resembles multilayer adsorption Fig. 5. The MOF-5 BJH pore sizes of 43 Å

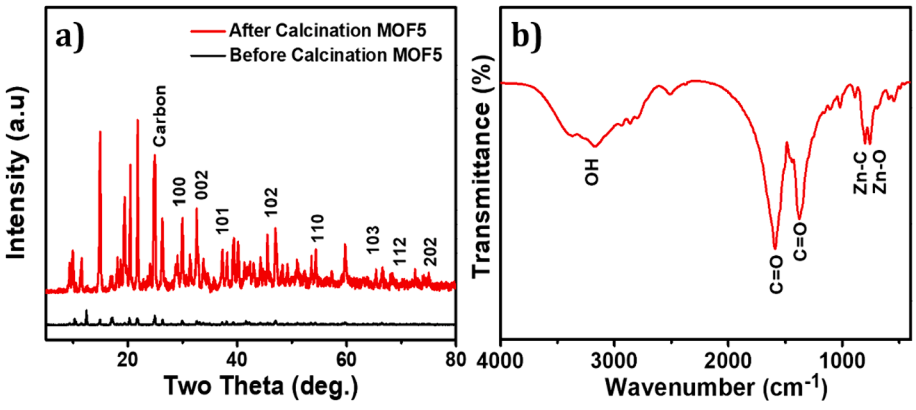

Fig. 2. A) x-ray diffraction pattern, and fourier transform infrared analysis of mof-5.

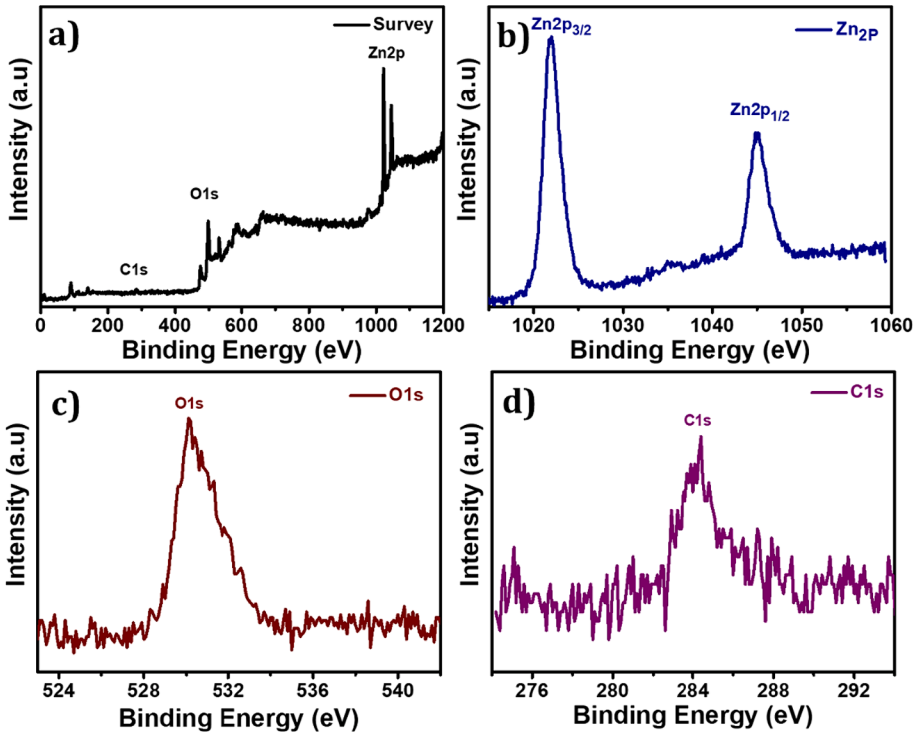

Fig. 3. XPS studies of MOF-5 (a) Survey spectrum, (b) High-resolution peak of Zn 2p3/2 (c) High-resolution peak of O1s, and (d) High-resolution peak of C1s.

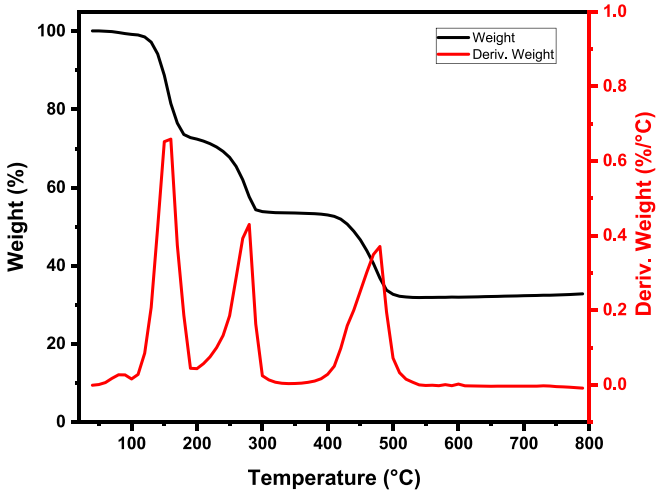

Fig. 4. Thermo-gravimetric analysis (TGA) graph of MOF-5.

further confirm the materials' mesoporous nature.

3.6. Electrochemical performance

The cyclic voltammetry of Zn-MOF working electrode examined in 3-electrode system at different scan rates in −0.6 V to 0.4 V potential window range as shown in Fig. 6a. The specific capacitance calculated by CV studies for Zn-MOF (Fig. 6b) decreased steadily from 341 to 191 F g^{-1} as the scan rate increased form 2–200 mV s^{-1}. Moreover, the performance of the material was also studied by performing GCD tests at various current densities 0.5 to 2.0 A g^{-1}, as showed in Fig. 6c. Moreover, specific capacitance was estimated by GCD curved and found enhanced values of specific capacitance ranging from 353 to 264 F g^{-1} at 0.5 to 2.0 A g^{-1} range. The highest value of specific capacitance Cs 353 F g^{-1} was found for lowest current density of 0.5 A g^{-1} as shown in Fig. 6d. An excellent cyclic stability was obtained after running 2000 cylic runs at a scan rate of 50 mV s^{-1} as demonstrated in Fig. 6e. The small semicircle of EIS plot exhibits superior electrochemical performance of the produced material as depicts in Fig. 6f.

4. Conclusion

In this work, we have used waste PET synthesized BDC to produce MOF5. MOF-5 or Zn-MOF were synthesized through a solvothermal route and phase, and purity was confirmed by powder x-ray studies. The particle diameter of MOF-5 was found in the range of 28.3–88.9 nm calculated through SEM micrographs. TEM images of MOF-5 crystals showed well-defined shapes of hexagonal, pyramidal, and spherical particles with an average size of 13.513–129.199 nm. The Nitrogen adsorption–desorption studies of MOF-5 samples show the type II isotherm with a BET surface area of 88 m^2 g^{-1}. Moreover, BJH pore size distribution shows the mesoporous nature of the produced MOF-5. An excellent specific capacitance ranging from 341 to 191 F g^{-1} recorded form the scan rate of 2–200 mV s^{-1} by CV for Zn-MOF. Moreover, the highest specific capacitance 353 F g^{-1} calculated at 0.5 A g^{-1} current density. The highest value of specific capacitance Cs 353 F g^{-1} was found for lowest current density of 0.5 A g^{-1}. An excellent cyclic stability was obtained after running 2000 cyclic runs at a scan rate of 50 mV s^{-1}. The small semicircle of EIS plot exhibits superior electrochemical performance of the Zn-MOF. The waste PET plastic derived Zn-MOF showed an excellent supercapacitor performance which can be utilized in energy storage applications as well as the use of waste PET plastic worked in environmental remediation.

CRediT authorship contribution statement

Abdullah M. Al-Enizi: Conceptualization, Data curation, Funding acquisition, Investigation, Methodology, Supervision, Validation, Writing – original draft, Writing – review & editing. **Ayman Nafady:** Data curation, Formal analysis, Investigation, Validation, Writing – review & editing. **Nouf B. Alanazi:** Conceptualization, Data curation,

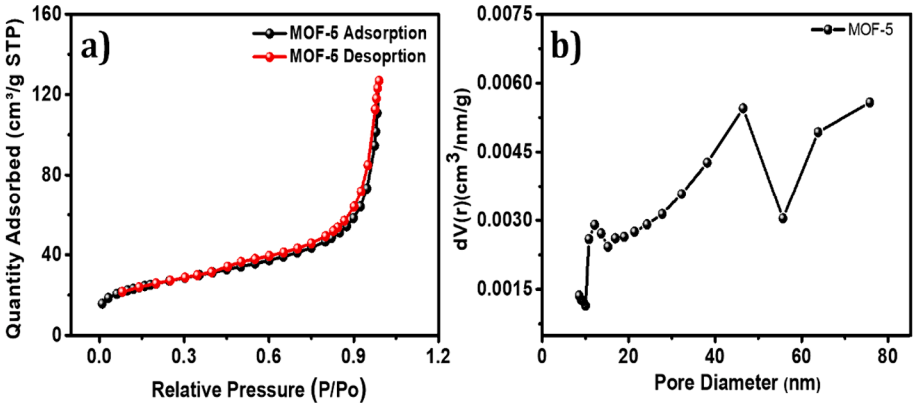

Fig. 5. (a) Nitrogen adsorption–desorption isotherm, and (b) BJH pore size distribution of MOF-5.

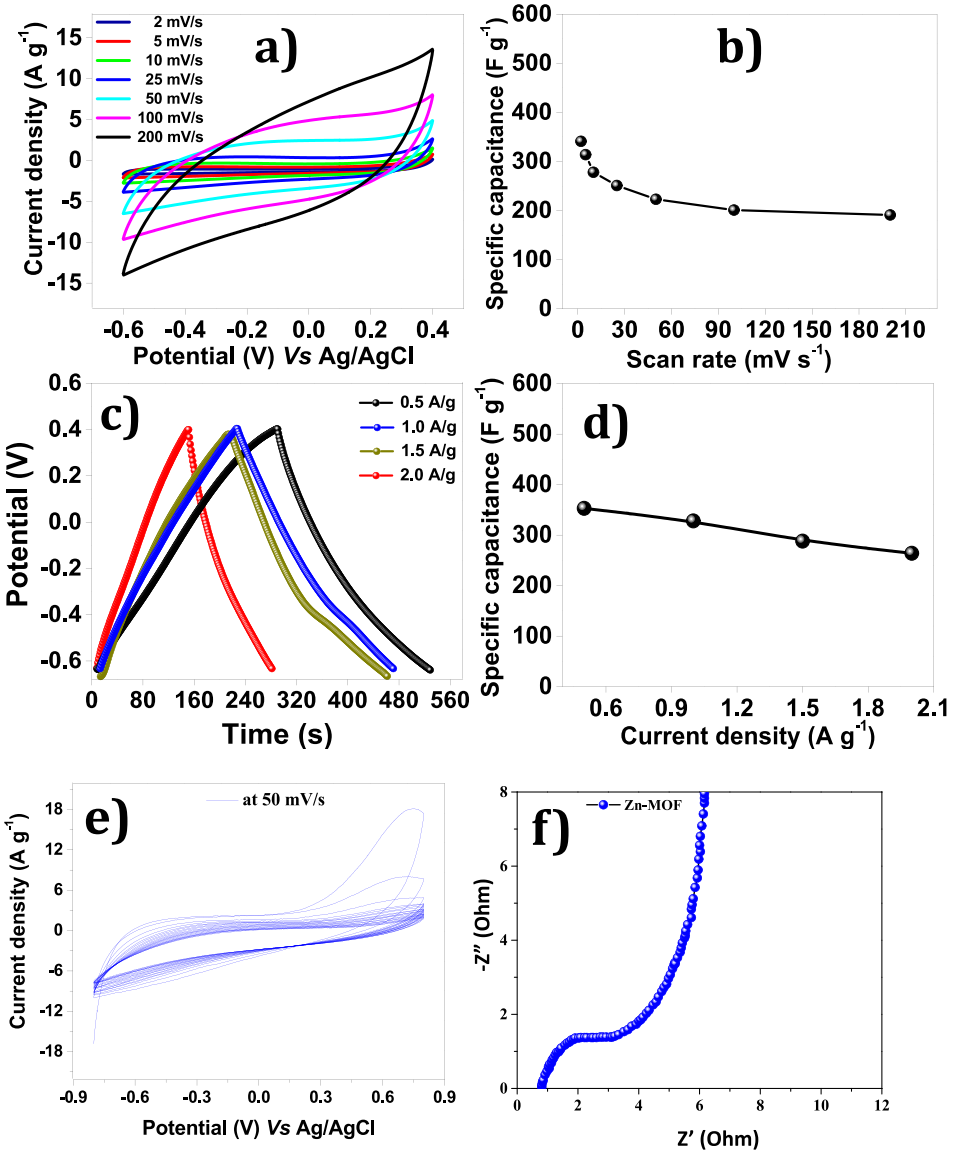

Fig. 6. Electrochemical performance of Zn-MOF (a) CV curves at different scan rates (b) Specific capacitance by CV (c) GCD curves at different current densities (d) Specific capacitance graph by GCD (e) Cyclic stability of Zn-MOF materials at 50 mV s^{-1} and (f) Nyquist plot.

Formal analysis, Validation, Writing – review & editing. **Meera Moydeen Abdulhameed:** Data curation, Formal analysis, Supervision, Validation, Writing – review & editing. **Shoyebmohamad F. Shaikh:** Conceptualization, Formal analysis, Methodology, Supervision, Writing – review & editing.

Declaration of competing interest

The authors declare that they have no known competing financial interests or personal relationships that could have appeared to influence the work reported in this paper.

Acknowledgment

The authors extend their appreciation to the Deputyship for Research & Innovation, "Ministry of Education" in Saudi Arabia for funding this research work through the project number (IFKSUDR_E167).

Appendix A. Supplementary data

Supplementary data to this article can be found online at https://doi.org/10.1016/j.jksus.2024.103179.

5. References

Al-Enizi, A.M., Ahmed, J., Ubaidullah, M., Shaikh, S.F., Ahamad, T., Naushad, M., Zheng, G., 2020. J. Clean. Prod. 248.
Al-Enizi, A.M., Ubaidullah, M., Ahmed, J., Ahamad, T., Ahmad, T., Shaikh, S.F., Naushad, M., 2020. Compos. Part B Eng. 183, 107655.
Al-Enizi, A.M., Ubaidullah, M., Ahmed, J., Ahamad, T., Ahmad, T., Shaikh, S.F., Naushad, M., 2020. Compos. Part B Eng. 183.
Annamalai, J., Murugan, P., Ganapathy, D., Nallaswamy, D., Atchudan, R., Arya, S., Khosla, A., Barathi, S., Sundramoorthy, A.K., 2022. Chemosphere 298, 134184.
Asadevi, H., Prasannakumaran Nair Chandrika Kumari, P., Padmavati Amma, R., Khadar, S.A., Charivumvasathu Sasi, S., Raghunandan, R., 2022. ACS Omega 7, 13031.
Asensio, M., Esfandiari, P., Núñez, K., Silva, J.F., Marques, A., Merino, J.C., Pastor, J.M., 2020. Compos. Part B Eng. 200, 108365.
Biserčić, M.S., Marjanović, B., Vasiljević, B.N., Mentus, S., Zasońska, B.A., Ćirić-Marjanović, G., 2019. Microporous Mesoporous Mater. 278, 23.
Cho, E., Yong Lee, S., Choi, J.-W., Kim, S.-H., Jung, K.-W., 2021. Sep. Purif. Technol. 279, 119719.
Deleu, W.P.R., Stassen, I., Jonckheere, D., Ameloot, R., De Vos, D.E., 2016. J. Mater. Chem. A 4, 9519.
Ding, Z., Hu, X., Yue, P.L., Lu, G.Q., Greenfield, P.F., 2001. Catal. Today 68, 173.
Gu, Z.-Y., Wang, G., Yan, X.-P., 2010. Anal. Chem. 82, 1365.
Iacomi, P., Gulcay-Ozcan, E., Pires Conti, P., Biswas, S., Steunou, N., Maurin, G., Rioland, G., Devautour-Vinot, S., 2022. ACS Appl. Mater. Interfaces 14, 17531.
Kandiah, M., Nilsen, M.H., Usseglio, S., Jakobsen, S., Olsbye, U., Tilset, M., Larabi, C., Quadrelli, E.A., Bonino, F., Lillerud, K.P., 2010. Chem. Mater. 22, 6632.
Kumar, G., Masram, D.T., 2021. ACS Omega 6, 9587.
Lewczuk, B., Szyryńska, N., 2021. Animals 11.
Li, J., Zhang, S., Hua, Y., Lin, Y., Wen, X., Mijowska, E., Tang, T., Chen, X., Ruoff, R.S., 2023. Green Energy Environ.
Lo, S.-H., Senthil Raja, D., Chen, C.-W., Kang, Y.-H., Chen, J.-J., Lin, C.-H., 2016. Dalt. Trans. 45, 9565.
Manju, P.K., Roy, A.R., Rajagopal, C., 2013. Mater. Lett. 106, 390.
Sarwar, B., Khan, A.U., Fazal, T., Aslam, M., Qaisrani, N.A., Ahmed, A., 2022. Sustainability 14.
Song, C., Zhang, B., Hao, L., Min, J., Liu, N., Niu, R., Gong, J., Tang, T., 2022. Green Energy Environ. 7, 411.
Sousa, A.F., Patrício, R., Terzopoulou, Z., Bikiaris, D.N., Stern, T., Wenger, J., Loos, K., Lotti, N., Siracusa, V., Szymczyk, A., Paszkiewicz, S., Triantafyllidis, K.S., Zamboulis, A., Nikolic, M.S., Spasojevic, P., Thiyagarajan, S., van Es, D.S., Guigo, N., 2021. Green Chem. 23, 8795.
Ubaidullah, M., Al-Enizi, A.M., Shaikh, S., Ghanem, M.A., Mane, R.S., 2020. J. King Saud Univ. - Sci. 32, 2397.
Ubaidullah, M., Al-Enizi, A.M., Ahamad, T., Shaikh, S.F., Al-Abdrabalnabi, M.A., Samdani, M.S., Kumar, D., Alam, M.A., Khan, M., 2021. J. Energy Storage 33, 102125.
Vellingiri, K., Tsang, D.C.W., Kim, K.-H., Deep, A., Dutta, T., Boukhvalov, D.W., 2018. J. Clean. Prod. 199, 995.
Volanti, M., Cespi, D., Passarini, F., Neri, E., Cavani, F., Mizsey, P., Fozer, D., 2019. Green Chem. 21, 885.
Xu, W., Dong, M., Di, L., Zhang, X., 2019. Nanomaterials 9.
Zhao, H., Song, H., Chou, L., 2012. Inorg. Chem. Commun. 15, 261.
Zorainy, M.Y., Sheashea, M., Kaliaguine, S., Gobara, M., Boffito, D.C., 2022. RSC Adv. 12, 9008.